

Towards a multi-core ultra-fast optical quantum processor: 43-GHz bandwidth real-time amplitude measurement of 5-dB squeezed light using modularized optical parametric amplifier with 5G technology

Asuka Inoue^{1*}, Takahiro Kashiwazaki¹, Taichi Yamashima², Naoto Takanashi², Takushi Kazama¹, Koji Enbutsu¹, Kei Watanabe¹, Takeshi Umeki¹, Mamoru Endo^{2,3} and Akira Furusawa^{2,3*}

¹NTT Device Technology Labs, NTT Corporation, 3-1, Morinosato Wakamiya, Atsugi, 243-0198, Kanagawa, Japan.

²Department of Applied Physics, School of Engineering, The University of Tokyo, 7-3-1, Hongo, Bunkyo, 113-8656, Tokyo, Japan.

³Optical Quantum Computing Research Team, RIKEN Center for Quantum Computing, 2-1, Hirosawa, Wako, 351-0198, Saitama, Japan.

*Corresponding author(s). E-mail(s):

asuka.inoue.hy@hco.ntt.co.jp; akiraf@ap.t.u-tokyo.ac.jp;

Contributing authors: takahiro.kashiwazaki.dy@hco.ntt.co.jp;
yamashima@alice.t.u-tokyo.ac.jp; takanashi@alice.t.u-tokyo.ac.jp;
takushi.kazama.me@hco.ntt.co.jp; koji.enbutsu.cm@hco.ntt.co.jp;
kei.watanabe.hg@hco.ntt.co.jp; takeshi.umeki.zv@hco.ntt.co.jp;
endo@ap.t.u-tokyo.ac.jp;

Abstract

Continuous-variable optical quantum information processing (CVOQIP), where quantum information is encoded in a traveling wave of light called a flying qubit, is a candidate for a practical quantum computer with high

clock frequencies. Homodyne detectors for quadrature-phase amplitude measurements have been the major factor limiting the clock frequency. Here, we developed a real-time amplitude measurement method using a modular optical parametric amplifier (OPA) and a broadband balanced photodiode that is commercially used for coherent wavelength-division multiplexing telecommunication of the fifth-generation mobile communication systems (5G). The OPA amplifies one quadrature-phase component of the quantum-level signal to a loss-tolerant macroscopic level, and acts as a “magic wand,” which the loss after the OPA is suppressed from 92.4% to only 0.4%. When the method was applied to a broadband squeezed vacuum with a center wavelength of 1545.32 nm, we observed 5.2 ± 0.5 dB of squeezing from DC to 43 GHz without any loss correction. The marriage of CVOQIP and 5G technology arranged by the modular OPA will lead to a paradigm shift from the conventional method of using stationary qubits, where the information is encoded in a standing wave system, to a method using flying qubits for ultra-fast practical quantum computation. This means that quantum computer research will move from the stage of developing machines that execute only specific quantum algorithms to a stage of developing machines that can outperform classical computers in running any algorithm.

Keywords: Optical quantum computer, Homodyne detection, Optical parametric amplifier

1 Introduction

Research on continuous-variable optical quantum information processing (CVOQIP), in which quantum information is encoded in an optical electromagnetic field, is aimed at realizing a fault-tolerant universal quantum computer [1–5]. This form of processing has a high carrier frequency, which can raise the upper limit of the clock frequency. Moreover, its decoherence is small even at room temperature and atmospheric pressure because the photon energy is high compare to the environment.

In CVOQIP, measurement-based quantum computation (MBQC) is a reasonable way of performing large-scale quantum computations [6, 7], rather than circuit-model computations. MBQC uses a cluster state as a resource state, which are special multipartite entangled states. The cluster state contains a superposition of all input-output relations in quantum computation, and can be regarded as superposition of quantum lookup tables. In order to select a desired input-output relation from them, that is, to perform the desired computation, we only need to perform local measurements for each qubit by collapsing the wavefunction. It is also called a one-way quantum computation because the measurements perform a quantum calculation and collapse the wavefunction simultaneously. It was initially proposed for a standing wave system, that is, stationary qubit [8]. In this case, the same qubit must be kept

until the calculation is completed, so the lifetime of the qubit, or its memory time, must be longer than the calculation time.

On the other hand, in the case of CVOQIP, the wave packets from the cluster state resource are treated as flying qubits [1]. Since homodyne detectors immediately measure each wave packet, the qubit is consumed, so there is no need to consider the lifetime [9, 10]. In other words, it can be called a one-pad quantum computation (OPQC).

The processor of an optical OPQC consists of a time-domain multiplexed (TDM) cluster state and a homodyne measurement that measures the quadrature-phase amplitude of each wave packet. The TDM cluster state is created on the basis of a continuous-wave (CW) squeezed vacuum [11–14]. In a squeezed vacuum, the noise of the electromagnetic field at a particular quadrature-phase component is below the vacuum. A squeezed vacuum is generated by creating quantum correlations between photons contained within a given period often through nonlinear optical processes such as parametric down conversion or four-wave mixing [15]. When two squeezed vacua are interfered with a beamsplitter, quantum entanglement is created between the two spatial modes at the output. The entanglement is time-delayed by an optical delay line and further passed through an asymmetric interferometer to extend the entanglement between time-different wave packets [6, 7].

The broader the squeezing bandwidth is, the shorter the quantum correlation time, defined by the inverse of the bandwidth of the squeezed vacuum, and the more wave packets can be “packed” per unit time. In other words, the upper limit of the clock frequency is the bandwidth of the squeezed vacuum. It has been reported that low-loss periodically poled lithium niobate (PPLN) waveguides can generate 6-dB of squeezing in a 6-THz bandwidth with a center wavelength of 1545 nm [16] and 4-dB squeezing in a 25-THz bandwidth with a center wavelength of 2 μm [17]. That is, a THz clock frequency can be realized in principle.

However, the bandwidth of the homodyne detectors f_{HD} and other devices is currently limited to about GHz, so the wide bandwidth of the squeezed vacuum is wasted, as depicted in Fig. 1 (a). To measure quantum light, the detection efficiency of a photodiode must be very high, but a photodiode specifically designed for this purpose will inevitably have a narrow bandwidth. Realistically, the bandwidth is limited to a few hundred MHz [18–20] or at best a few GHz with state-of-the-art silicon photonics technology [21, 22].

Recently, a technique employing an optical parametric amplifier (OPA) has been used to measure a broadband squeezed vacuum [17, 23, 24]. OPAs act as phase-sensitive optical amplifiers that can amplify one quadrature-phase component without adding noise, i.e., with a noise figure (NF) of 0 dB in principle [25–27]. This is a significant difference from phase-insensitive optical amplifiers (e.g., erbium-doped fiber amplifiers, Raman amplifiers, semiconductor optical amplifiers, etc.), which cannot cross the $\text{NF} = 3$ dB barrier [25]. A quantum-level signal can be converted into a macroscopic level with a low-loss OPA with a sufficiently high gain acting as an optical pre-amplifier

for quantum measurements [28]. Consequently, optical losses and electrical noise are suppressed, which significantly increase the degrees of freedom of the measuring instrument. However, the previous studies made only narrow bandwidth measurements or power measurements like spectrum analyzers [17, 23, 24], while OPQC requires real-time broadband quadrature-phase amplitude measurements made by homodyne detectors.

In this paper, an OPA amplified one quadrature-phase component of the light to be measured, then we detected its output with a balanced photodiode and a broadband amplifier. The OPA acts as an optical pre-amplifier and suppresses the losses after the OPA from 92.4% to only 0.4%, yielding an overall homodyne measurement system efficiency of 79%. We measured a broadband squeezed vacuum with a center frequency of 194.0 THz (wavelength of 1545.32 nm) generated by another OPA [16]. We observed 5.2-dB squeezing in the band from near DC to 43 GHz without any loss correction. Thus this method can overcome the loss problem, which is the main concern in the field of silicon-photonics based quantum information processing.

The critical component of this work is a fiber-coupled, low-loss and high-gain broadband OPA with a PPLN waveguide. Many of the other components are commonly used in digital coherent telecommunications in the fifth-generation mobile communication systems (5G). We believe that the resulting marriage of CVOQIP and 5G technology will lead directly to an optical quantum computer with a clock frequency exceeding 40 GHz. The 5G elements used in our demonstration were the balanced photodiodes and an electrical amplifier. In addition, as illustrated in Fig. 1 (b), dividing the bandwidth of the squeezed vacuum using dense wavelength division multiplexing (DWDM), as is done in WDM digital coherent communications, enables multiple independent quantum processors to be realized from a single light source. In this case, optical quantum computer can be realized by applying a high-repetition-rate optical frequency comb to the phase-coherent local oscillator light for each homodyne detector.

2 Results

2.1 Homodyne detection with OPA

The electromagnetic field of light with a carrier frequency of ω_0 is represented by using annihilation and creation operators, $\hat{A}(t)$ and $\hat{A}^\dagger(t)$, excluding the oscillation term associated with the carrier frequency, as follows:

$$\hat{E}(z, t) \propto \hat{A}(t)e^{i(kz - \omega_0 t)} + \hat{A}^\dagger(t)e^{-i(kz - \omega_0 t)} \quad (1)$$

$$= \sqrt{2} \left(\hat{X}(t) \cos(kz - \omega_0 t) + \hat{P}(t) \sin(kz - \omega_0 t) \right). \quad (2)$$

Here, these operators satisfy the commutation relation $[\hat{A}(t), \hat{A}^\dagger(t')] = \delta(t - t')$, where $\delta(t)$ is the Kronecker delta function, and $\hat{X}(t) \equiv \frac{\hat{A}(t) + \hat{A}^\dagger(t)}{\sqrt{2}}$, $\hat{P}(t) \equiv$

$\frac{\hat{A}(t) - \hat{A}^\dagger(t)}{\sqrt{2i}}$ are called the quadrature-phase amplitude operators. We often consider wavepackets of light defined by a temporal mode function $f(t)$ as $\hat{A}_f(t) \equiv \int dt' f(t' - t) \hat{A}(t')$, and the quadrature-phase amplitude operators of this mode are defined as $\hat{X}_f(t) \equiv \frac{\hat{A}_f(t) + \hat{A}_f^\dagger(t)}{\sqrt{2}}$, $\hat{P}_f(t) \equiv \frac{\hat{A}_f(t) - \hat{A}_f^\dagger(t)}{\sqrt{2i}}$. Figure 1 (c) shows examples of measurement results which correspond to eigenvalues $X_f(t)$ and $P_f(t)$ of $\hat{X}_f(t)$ and $\hat{P}_f(t)$, respectively.

When we perform balanced homodyne detection using local oscillator (LO) light with an optical frequency of ω_0 as shown in Fig. 1 (d) and (e), the output can be written as

$$\hat{I}_{\text{HD}}(t, \theta) \propto \hat{X}_{\text{HD}}(t) \cos \theta + \hat{P}_{\text{HD}}(t) \sin \theta \quad (3)$$

$$\hat{X}_{\text{HD}}(t) \equiv \int dt' f_{\text{HD}}(t' - t) \hat{X}_f(t') \quad (4)$$

$$\hat{P}_{\text{HD}}(t) \equiv \int dt' f_{\text{HD}}(t' - t) \hat{P}_f(t'), \quad (5)$$

where θ is the phase between the signal and LO lights, and it is assumed that the LO light is sufficiently strong and the quantum fluctuations are negligible. f_{HD} is the temporal mode function of the instruments, including the homodyne detector, amplifiers, filters, oscilloscope and so on. The Fourier transform of $f_{\text{HD}}(t)$ is related to the frequency response of the measurement system. For CVOQIP fields, the time-domain data are used not only to read the result but also to process the signal by using feedforward operations.

For example, a homodyne detector with high detection efficiency ($\eta_{\text{HD}} \sim 1$) is typically used in the case of a standard homodyne system for measuring the quantum state of light (Fig. 1 (d)). Several research groups have used this kind of system to measure high-level squeezed vacua [18–20] or non-Gaussian states with strong Wigner negativity, such as Schrödinger cats [29–32] or photon-number states [33, 34]. However, such a homodyne system is specialized for achieving high-detection efficiency, and the bandwidth is not very wide (typically less than GHz order).

In contrast, broadband balanced detectors lift the bandwidth beyond a GHz or even higher. Recently, GHz homodyne detectors built with silicon photonics technology [21, 22] have been demonstrated; one of them measured a broadband squeezed vacuum [21]. Nevertheless, to increase the bandwidth, it is necessary to use photodiodes with a thin active layer and a small photosensitive area, which is not suitable for achieving high detection efficiency. Although the coupling efficiency can be increased by integration, there are still limitations. Losses and electrical noises directly degrade the signal-to-noise ratio (SNR) of the homodyne system, which is critical for CVOQIP applications (Fig. 1 (e)).

Here, we amplify the X component by using an OPA and detect the output with a homodyne detector, as depicted in Fig. 1 (f). The output signal is

represented as

$$\hat{I}_{\text{HD,OPA}}(t, \theta) \propto \sqrt{G} \hat{X}_{\text{HD}}(t) \cos \theta + \frac{1}{\sqrt{G}} \hat{P}_{\text{HD}}(t) \sin \theta, \quad (6)$$

where G is the gain of the OPA. Instead of losing information in the P component, the X component is amplified, as shown in Fig. 1 (f). By setting $\theta = 0$, the X component of the quadrature-phase amplitude can be measured. The ideal OPA acts as a phase-sensitive optical amplifier and does not add noise when amplifying the X component, thus suppressing the loss of the broadband homodyne detector.

Let the efficiencies of the homodyne detector and OPA be η_{HD} and η_{OPA} , respectively. The effective efficiency of the system can be written as

$$\eta_{\text{eff}} = \frac{\eta_{\text{OPA}} \eta_{\text{HD}}}{\eta_{\text{HD}} + \frac{1 - \eta_{\text{HD}}}{G}}. \quad (7)$$

From this expression, if the loss of the OPA is small compared with the loss of the homodyne detector and the gain of the OPA is sufficiently high, $G \gg 1$, the OPA can suppress for the loss of the homodyne detector (see Methods). Optical losses, the detection efficiency of a broadband balanced photodiode, and electrical noise in the broadband measurement equipment would easily increase the total loss of the homodyne system to more than 90%, corresponds to $\eta_{\text{HD}} = 10\%$. Consider, for example, a case where the loss is 90% ($\eta_{\text{HD}} = 10\%$): if the OPA has a gain G of 35 dB and an efficiency η_{OPA} of 79% (corresponds to 1-dB NF), the loss after the OPA can be improved from 90% to only 0.3%. Moreover, further improvements in efficiency could be achieved in the future if a low-loss and high-gain OPA could be realized.

2.2 Experimental apparatus

Figure 2 (a) shows the experimental apparatus of our homodyne system. The fundamental light is from a continuous-wave fiber laser (NKT photonics, X15) at 1545.32 nm (not shown). The light to be measured is a broadband squeezed vacuum generated by a fiber pig-tailed OPA (OPA 1 in the figure) [16]. The output fiber of OPA 1 is connected to the input fiber of OPA 2 (used as a phase-sensitive optical amplifier), which is excited by pump light with a wavelength of 773 nm. 10% of the OPA2 output is used for monitoring the output spectrum by an optical spectrum analyzer (OSA, Yokogawa AQ6370D), and locking the phase between the squeezed vacuum and the sub harmonic of the pump light by a feedback circuit (FBC1) [24] (see the supplementary information). The remaining 90% is sent to a 50:50 fiber beamsplitter, where it interferes with the local oscillator (LO) light and is received by a balanced photodiode (BD, u²t, BPDV21x0R). Delay lines (DLs) and variable optical attenuators (VOAs) are inserted in each path to adjust the optical path length and power balance. The two photodiodes are reverse biased by biasing circuits, and each photocurrent I_{PD} is monitored (not shown). The output of the

balanced photodiode is amplified by a broadband amplifier (AMP, SHF, S807 B, 55-GHz bandwidth). The output is split by a broadband power splitter (SPL, Anritsu, W241A); then, one part is measured by a real-time oscilloscope (Keysight, DSO-Z 634A, 63-GHz analog bandwidth). The other part is monitored by an electrical spectrum analyzer (ESA, Keysight, EXA N9010B). The ESA is also used to generate an error signal to lock the phase between the LO light and the output of OPA 2 by a feedback circuit (FBC 2) (see the supplementary information for details).

2.3 Characterization of the homodyne system

In the following experiments, the pump power of OPA2 was set to 1.2 W. The parametric gain G and NF of OPA2 were 35 dB and 1 dB, respectively (see the supplementary information and the reference [27]). The measured loss after the OPA2 was 92.4%, then from Eq.7 the effective efficiency of the total homodyne system is 79%. Figure 2 (b) shows the raw data of the homodyne detector. The black trace shows the electrical noise floor when all the light is blocked. The red trace shows the shot noise with the LO when the photocurrent of each photodiode is set to 3.0 mA. We acquired the output signal for 78.2 ns. Figure 2 (c) shows fast Fourier transform (FFT) traces of the acquired data with different LO powers. These traces were calculated by averaging the results of 8192 measurements taken over a 0.8-ms period and all the frequency response traces are averaged for 8192 traces. The traces show a flat frequency response up to 10 GHz. The 3-dB bandwidth of our system is 43 GHz of the BD, and even at that frequency, 20 dB of SNR is obtained when the photocurrent is 3.0 mA (red trace). All the traces are fall off beyond the frequency of 63 GHz, which is the the edge of the oscilloscope's bandwidth. Note that OPA 2 has a THz bandwidth, which means a much wider bandwidth can be obtained if faster electronics can be used.

2.4 Measurement of broadband squeezed light

Figure 3 (a) shows the raw data corresponding to quadrature-phase amplitudes of the squeezed light of the anti-squeezing and squeezing components (left and right, respectively). The center shows the shot noise when the pump for OPA 1 is set to 0 mW. Figure 3 (b) is a histogram based on the measurement results of Fig. 3 (a). Figure 3 (a) and (b) clearly show quadrature squeezing of the light to be measured.

The FFTs of these data are shown in Fig. 3 (c), and the normalized squeezing level calculated for several pump powers of OPA 1 is shown in Fig. 3 (d). From these figures, it can be seen that the homodyne system successfully measured a 5.2-dB broadband squeezed vacuum from DC to 43 GHz. Note that the peaks at 34 GHz are measurement artifacts caused by the oscilloscope.

Figure 3 (e) shows the squeezing and anti-squeezing levels as the function of pump power for OPA 1. The occupied circles are calculated from the variance of time-domain data like in Fig. 3 (a), and the error bars are estimated from

8192 data sets. For a pump power of 438 mW, a squeezing level of 5.2 ± 0.5 dB and an anti-squeezing level of 13.9 ± 0.1 dB are obtained. The dashed line is the fitting to the function:

$$R_{\pm}(P) = L + (1 - L) \exp\left(\pm 2\sqrt{aP}\right) \quad (8)$$

where \pm represents anti-squeezing (+, blue) or squeezing (-, red), L represents the total effective loss of the system, including of OPA 1 and the homodyne system, and a is a second-harmonic-generation coefficient in the unit of W^{-1} . The fitting result shows the system loss of 29%, including losses of OPA 1, OPA 2, optical propagation, detector, and the electrical noise of the instruments. This value limits the squeezing level that can be measured with this apparatus to 5.2 dB.

In order to confirm the performance of the suppressing losses after OPA2, we inserted a VOA (not shown in Fig. 2 (a)) after OPA2 to worsen η_{HD} and measured the squeezing level as a function of the loss as shown in Fig. 3 (f). Note that the measurements in Fig. 3 (f) are not broadband measurements by the oscilloscope but rather narrowband measurements made with ESA at a sideband frequency of 100 MHz and we did not lock the LO phase (see supplementary information). The dashed and solid lines are calculated traces when $G = 0$ and 35 dB. The markers with error bars represent the measured values. It is clear from this figure that OPA2 with $G = 35$ dB effectively suppresses the loss after OPA2 from 92.4% to 0.4%, and the system can measure the original squeezing level.

3 Discussion

The most significant advantage of optical quantum computers is that the upper limit of the clock frequency is by far the highest compared with other methods. The bandwidth of the squeezed light used to generate the cluster states is above THz, meaning that a THz-clocked quantum computer can be realized in principle. However, the bandwidth on the measurement instruments, including the homodyne detectors, has not kept pace, and a large part of the bandwidth of the squeezed light is wasted. We have experimentally demonstrated a high-detection efficiency (79%) and wide-bandwidth (43 GHz) homodyne system using an OPA module and commercially available 5G components. The OPA drastically suppress the losses after OPA2 from 92.4% to only 0.4%. With this system, we performed real-time measurements of the quadrature-phase amplitude of broadband squeezed vacuum, obtaining a squeezing level of 5.2 ± 0.5 dB without loss correction. This value exceeds one of the thresholds (4.5 dB) for cluster state generation [13], indicating that this method can be applied to quantum calculations. In fact, except for the handling of non-Gaussian quantum states [4, 35], the necessary elements for optical quantum computation are LO phase switching and feedforward systems, which are parts of classical information processing. Even at present, there are electro-optical modulators

and electronics above 40 GHz in bandwidth as 5G technology [36, 37], and when “Beyond 5G” or 6G technologies [38] appear in the future, the speed of classical information processing will be further increased. This means that the broadband homodyne detector developed in this study will make it feasible for the clock frequency of optical quantum computers to exceed 40 GHz.

We conclude this paper by proposing a multi-core optical quantum processor by effectively using the full-bandwidth of squeezed vacuum with our homodyne system.

Quantum entanglement between two frequency sidebands is the essential feature of a squeezed vacuum. In this study, we measured the quantum correlation in the ± 43 GHz bandwidth around a frequency f_c of 194.0 THz, as shown in Fig. 1 (a). Therefore, by dividing the optical spectrum into frequency-band pairs with DWDM (e.g., with a frequency spacing $\Delta f = 100$ GHz) and applying our homodyne system for each as illustrated in Fig. 1 (b), a multi-core optical quantum processor can be realized, wherein the operating clock of each processor exceeds 40 GHz. As well, optical frequency comb technology can be used to prepare phase-coherent LO beams for each homodyne system [39, 40]. This research shows that CVOQIP is highly compatible with mature 5G technology.

Increasing the clock frequency and core multiplexing technologies have dramatically enhanced the processing speed of classical computers, which created the current information society. The method proposed in this paper shows that high-clock frequency and multi-cores are also possible in optical quantum computers. Ultra-fast multi-core optical quantum processors will catapult quantum computer research into a new era, where versatile quantum computers surpass classical computers in any algorithm, not just in specific quantum algorithms.

4 Methods

4.1 OPAs

We used two kinds of OPA. Both are 45-mm-long, ZnO-doped PPLN waveguides, but their fabrication processes and waveguide structures are different. This is because their different applications require modules with different characteristics. OPA 1, which is used for generating the broadband squeezed vacuum, is fabricated by mechanically polishing and the thickness and the width of the waveguide are about $8\text{ }\mu\text{m}$ and $8.6\text{ }\mu\text{m}$. Thanks to the smooth surface and relatively large waveguide core, the waveguide loss is only 7% and even the total loss of the fiber pig-tailed module is only 21%, which is an appropriate level for generating squeezed vacuum. In contrast, the parametric gain of this module is not very high (~ 15 dB when the pump power of 438 mW).

In contrast, OPA 2 is fabricated by a chemical etching process, and its thickness and width are about $5\text{ }\mu\text{m}$ and $5.6\text{ }\mu\text{m}$. Because the waveguide is relatively smaller than the one of OPA 1, the loss is slightly higher, but a

parametric gain of 35 dB can be obtained for a pump power of 1.2 W. See the references for more details (OPA 1 [16], OPA 2 [27, 41]).

4.2 Effective efficiency

Equation 7 can be re-written as follows with efficiencies when $\theta = 0$:

$$\begin{aligned} \hat{I}_{\text{HD,OPA}}(t, 0) \propto & \sqrt{\eta_{\text{HD}}\eta_{\text{OPA}}G}\hat{X}_{\text{HD}}(t) \\ & + \sqrt{\eta_{\text{HD}}(1 - \eta_{\text{OPA}})G}\hat{X}_{\text{vac,OPA}}(t) + \sqrt{1 - \eta_{\text{HD}}}\hat{X}_{\text{vac,HD}}(t), \end{aligned} \quad (9)$$

where $\hat{X}_{\text{vac,OPA}}(t)$ and $\hat{X}_{\text{vac,HD}}(t)$ are the quadrature-phase amplitude of the vacuum due to the losses. From this equation, the effective efficiency η_{eff} is calculated as

$$\eta_{\text{eff}} = \frac{\eta_{\text{HD}}\eta_{\text{OPA}}G}{\eta_{\text{HD}}\eta_{\text{OPA}}G + \eta_{\text{HD}}(1 - \eta_{\text{OPA}})G + (1 - \eta_{\text{HD}})} \quad (10)$$

$$= \frac{\eta_{\text{OPA}}\eta_{\text{HD}}}{\eta_{\text{HD}} + \frac{1 - \eta_{\text{HD}}}{G}} \quad (11)$$

$$\xrightarrow{G \rightarrow \infty} \eta_{\text{OPA}}. \quad (12)$$

5 Data availability

Data are available from the authors upon request.

6 Acknowledgments

The authors acknowledge supports from the UTokyo Foundation and donations from Nichia Corporation of Japan. T.Y. acknowledges support from the Advanced Leading Graduate Course for Photon Science (ALPS). M.E. acknowledges support from the Research Foundation for OptoScience and Technology. This work was partly supported by the Japan Science and Technology Agency (JPMJMS2064) and the Japan Society for the Promotion of Science KAKENHI (18H05207, 20K15187). The authors acknowledge Dr. Hiroshi Yamazaki for supporting the setup of the broadband detection system, and Mr. Takeru Ebihara for fruitful discussion.

7 Author contributions

A.I. N.T., and T.U. conceived and planned the project. A.I., T. Kashiwazaki, T.Y. and T.U. designed and constructed the experimental apparatus and acquired the data. T. Kashiwazaki, T. Kazama, K.E., K.W., and T.U. developed the low-noise and high-gain OPA module. A.I., T. Kashiwazaki, and M.E. analyzed the data and wrote the manuscript with assistance from all other co-authors. A.F. supervised the project.

8 Competing interests

The authors declare no competing financial interests.

References

- [1] Lloyd, S., Braunstein, S.L.: Quantum computation over continuous variables. *Physical Review Letters* **82**(8), 1784–1787 (1999) [arXiv:9810082](#) [quant-ph]. <https://doi.org/10.1103/PhysRevLett.82.1784>
- [2] O’Brien, J.L., Furusawa, A., Vučković, J.: Photonic quantum technologies (2009). <https://doi.org/10.1038/nphoton.2009.229>
- [3] Takeda, S., Furusawa, A.: Toward large-scale fault-tolerant universal photonic quantum computing. *APL Photonics* **4**(6), 060902 (2019) [arXiv:1904.07390](#). <https://doi.org/10.1063/1.5100160>
- [4] Fukui, K., Takeda, S.: Building a large-scale quantum computer with continuous-variable optical technologies. *Journal of Physics B: Atomic, Molecular and Optical Physics* (2022) [arXiv:2110.03247](#). <https://doi.org/10.1088/1361-6455/ac489c>
- [5] Asavanant, W., Furusawa, A.: *Optical Quantum Computers A Route to Practical Continuous Variable Quantum Information Processing*. AIP Publishing, Melville, New York (2022). <https://doi.org/10.1063/9780735424074>. <https://aip.scitation.org/doi/pdf/10.1063/9780735424074>
- [6] Menicucci, N.C.: Temporal-mode continuous-variable cluster states using linear optics. *Physical Review A* **83**(6), 062314 (2011) [arXiv:1007.3434](#). <https://doi.org/10.1103/PhysRevA.83.062314>
- [7] Ukai, R.: *Multi-Step Multi-Input One-Way Quantum Information Processing with Spatial and Temporal Modes of Light*. Springer Theses. Springer, Tokyo (2015). <https://doi.org/10.1007/978-4-431-55019-8>. <http://link.springer.com/10.1007/978-4-431-55019-8>
- [8] Raussendorf, R., Briegel, H.J.: A one-way quantum computer. *Physical Review Letters* **86**(22), 5188–5191 (2001). <https://doi.org/10.1103/PhysRevLett.86.5188>
- [9] Asavanant, W., Charoensombutamon, B., Yokoyama, S., Ebihara, T., Nakamura, T., Alexander, R.N., Endo, M., Yoshikawa, J., Menicucci, N.C., Yonezawa, H., Furusawa, A.: Time-Domain-Multiplexed Measurement-Based Quantum Operations with 25-MHz Clock Frequency. *Physical Review Applied* **16**(3), 1 (2021). <https://doi.org/10.1103/PhysRevApplied.16.034005>

- [10] Larsen, M.V., Guo, X., Breum, C.R., Neergaard-Nielsen, J.S., Andersen, U.L.: Deterministic multi-mode gates on a scalable photonic quantum computing platform. *Nature Physics* **17**(9), 1018–1023 (2021). <https://doi.org/10.1038/s41567-021-01296-y>
- [11] Yokoyama, S., Ukai, R., Armstrong, S.C., Sornphiphatphong, C., Kaji, T., Suzuki, S., Yoshikawa, J., Chi, Yonezawa, H., Menicucci, N.C., Furusawa, A.: Ultra-large-scale continuous-variable cluster states multiplexed in the time domain. *Nature Photonics* **7**(12), 982–986 (2013) [arXiv:1306.3366](https://arxiv.org/abs/1306.3366). <https://doi.org/10.1038/nphoton.2013.287>
- [12] Yoshikawa, J., Yokoyama, S., Kaji, T., Sornphiphatphong, C., Shiozawa, Y., Makino, K., Furusawa, A.: Invited Article: Generation of one-million-mode continuous-variable cluster state by unlimited time-domain multiplexing. *APL Photonics* **1**(6), 060801 (2016) [arXiv:1606.06688](https://arxiv.org/abs/1606.06688). <https://doi.org/10.1063/1.4962732>
- [13] Asavanant, W., Shiozawa, Y., Yokoyama, S., Charoensombutamon, B., Emura, H., Alexander, R.N., Takeda, S., Yoshikawa, J., Menicucci, N.C., Yonezawa, H., Furusawa, A.: Generation of time-domain-multiplexed two-dimensional cluster state. *Science* **366**(6463), 373–376 (2019). <https://doi.org/10.1126/science.aay2645>
- [14] Larsen, M.V., Guo, X., Breum, C.R., Neergaard-Nielsen, J.S., Andersen, U.L.: Deterministic generation of a two-dimensional cluster state. *Science* **366**(6463), 369–372 (2019). <https://doi.org/10.1126/science.aay4354>
- [15] Andersen, U.L., Gehring, T., Marquardt, C., Leuchs, G.: 30 Years of Squeezed Light Generation. *Physica Scripta* **91**(5) (2016) [arXiv:1511.03250](https://arxiv.org/abs/1511.03250). <https://doi.org/10.1088/0031-8949/91/5/053001>
- [16] Kashiwazaki, T., Yamashima, T., Takanashi, N., Inoue, A., Umeki, T., Furusawa, A.: Fabrication of low-loss quasi-single-mode PPLN waveguide and its application to a modularized broadband high-level squeezer. *Applied Physics Letters* **119**(25) (2021). <https://doi.org/10.1063/5.0063118>
- [17] Nehra, R., Sekine, R., Ledezma, L., Guo, Q., Gray, R.M., Roy, A., Marandi, A.: Few-cycle vacuum squeezing in nanophotonics. *arXiv* (2022) [arXiv:2201.06768](https://arxiv.org/abs/2201.06768)
- [18] Mehmet, M., Ast, S., Eberle, T., Steinlechner, S., Vahlbruch, H., Schnabel, R.: Squeezed light at 1550 nm with a quantum noise reduction of 123 dB. *Optics Express* **19**(25), 25763 (2011). <https://doi.org/10.1364/OE.19.025763>

- [19] Huang, D., Fang, J., Wang, C., Huang, P., Zeng, G.H.: A 300-MHz bandwidth balanced homodyne detector for continuous variable quantum key distribution. *Chinese Physics Letters* **30**(11) (2013). <https://doi.org/10.1088/0256-307X/30/11/114209>
- [20] Vahlbruch, H., Mehmet, M., Danzmann, K., Schnabel, R.: Detection of 15 dB Squeezed States of Light and their Application for the Absolute Calibration of Photoelectric Quantum Efficiency. *Physical Review Letters* **117**(11), 1–5 (2016). <https://doi.org/10.1103/PhysRevLett.117.110801>
- [21] Tasker, J.F., Frazer, J., Ferranti, G., Allen, E.J., Brunel, L.F., Tanzilli, S., D’Auria, V., Matthews, J.C.F.: Silicon photonics interfaced with integrated electronics for 9 GHz measurement of squeezed light. *Nature Photonics* (2020). <https://doi.org/10.1038/s41566-020-00715-5>
- [22] Bruynsteen, C., Vanhoecke, M., Bauwelinck, J., Yin, X.: Integrated balanced homodyne photonic–electronic detector for beyond 20 GHz shot-noise-limited measurements. *Optica* **8**(9), 1146 (2021). <https://doi.org/10.1364/OPTICA.420973>
- [23] Shaked, Y., Michael, Y., Vered, R.Z., Bello, L., Rosenbluh, M., Pe’er, A.: Lifting the bandwidth limit of optical homodyne measurement with broadband parametric amplification. *Nature communications* **9**(1), 609 (2018). <https://doi.org/10.1038/s41467-018-03083-5>
- [24] Takanashi, N., Inoue, A., Kashiwazaki, T., Kazama, T., Enbutsu, K., Kasahara, R., Umeki, T., Furusawa, A.: All-optical phase-sensitive detection for ultra-fast quantum computation. *Optics Express* **28**(23), 34916 (2020) [arXiv:2008.08216](https://arxiv.org/abs/2008.08216). <https://doi.org/10.1364/oe.405832>
- [25] Caves, C.M.: Quantum limits on noise in linear amplifiers. *Physical Review D* **26**(8), 1817–1839 (1982). <https://doi.org/10.1103/PhysRevD.26.1817>
- [26] Umeki, T., Tadanaga, O., Takada, A., Asobe, M.: Phase sensitive degenerate parametric amplification using directly-bonded PPLN ridge waveguides. *Optics Express* **19**(7), 6326 (2011). <https://doi.org/10.1364/OE.19.006326>
- [27] Kazama, T., Umeki, T., Shimizu, S., Kashiwazaki, T., Enbutsu, K., Kasahara, R., Miyamoto, Y., Watanabe, K.: Over-30-dB gain and 1-dB noise figure phase-sensitive amplification using a pump-combiner-integrated fiber I/O PPLN module. *Optics Express* **29**(18), 28824 (2021). <https://doi.org/10.1364/oe.434601>
- [28] Manceau, M., Leuchs, G., Khalili, F., Chekhova, M.: Detection Loss Tolerant Supersensitive Phase Measurement with an SU(1,1) Interferometer.

- Physical Review Letters **119**(22), 1–5 (2017) [arXiv:1705.02662](https://arxiv.org/abs/1705.02662). <https://doi.org/10.1103/PhysRevLett.119.223604>
- [29] Neergaard-Nielsen, J.S., Nielsen, B.M., Hettich, C., Mølmer, K., Polzik, E.S.: Generation of a superposition of odd photon number states for quantum information networks. Physical Review Letters **97**(8), 1–4 (2006) [arXiv:0602198](https://arxiv.org/abs/0602198) [quant-ph]. <https://doi.org/10.1103/PhysRevLett.97.083604>
 - [30] Gerrits, T., Glancy, S., Clement, T.S., Calkins, B., Lita, A.E., Miller, A.J., Migdall, A.L., Nam, S.W., Mirin, R.P., Knill, E.: Generation of optical coherent-state superpositions by number-resolved photon subtraction from the squeezed vacuum. Physical Review A **82**(3), 031802 (2010). <https://doi.org/10.1103/PhysRevA.82.031802>
 - [31] Asavanant, W., Nakashima, K., Shiozawa, Y., Yoshikawa, J.-I., Furusawa, A.: Generation of highly pure Schrödinger’s cat states and real-time quadrature measurements via optical filtering. Optics Express **25**(26), 32227–32242 (2017) [arXiv:1708.04042](https://arxiv.org/abs/1708.04042). <https://doi.org/10.1364/oe.25.032227>
 - [32] Takase, K., Kawasaki, A., Jeong, B.K., Endo, M., Kashiwazaki, T., Kazama, T., Enbutsu, K., Watanabe, K., Umeki, T., Miki, S., Terai, H., Yabuno, M., China, F., Asavanant, W., Yoshikawa, J.-i., Furusawa, A.: Generation of Schrödinger cat states with Wigner negativity using a continuous-wave low-loss waveguide optical parametric amplifier. Optics Express **30**(9), 14161 (2022) [arXiv:2201.06185](https://arxiv.org/abs/2201.06185). <https://doi.org/10.1364/oe.454123>
 - [33] Neergaard-Nielsen, J.S., Nielsen, B.M., Takahashi, H., Vistnes, A.I., Polzik, E.S.: High purity bright single photon source. Optics Express **15**(13), 7940 (2007). <https://doi.org/10.1364/OE.15.007940>
 - [34] Yukawa, M., Miyata, K., Mizuta, T., Yonezawa, H., Marek, P., Filip, R., Furusawa, A.: Generating superposition of up-to three photons for continuous variable quantum information processing. Optics Express **21**(5), 5529–5535 (2013). <https://doi.org/10.1364/OE.21.005529>
 - [35] Gottesman, D., Kitaev, A., Preskill, J.: Encoding a qubit in an oscillator. Physical Review A. Atomic, Molecular, and Optical Physics **64**(1), 123101–1231021 (2001). <https://doi.org/10.1103/PhysRevA.64.012310>
 - [36] Wang, C., Zhang, M., Chen, X., Bertrand, M., Shams-Ansari, A., Chandrasekhar, S., Winzer, P., Lončar, M.: Integrated lithium niobate electro-optic modulators operating at CMOS-compatible voltages. Nature **562**(7725), 101–104 (2018). <https://doi.org/10.1038/s41586-018-0551-y>

- [37] Xu, M., Zhu, Y., Pittalà, F., Tang, J., He, M., Ng, W.C., Wang, J., Ruan, Z., Tang, X., Kuschnerov, M., Liu, L., Yu, S., Zheng, B., Cai, X.: Dual-polarization thin-film lithium niobate in-phase quadrature modulators for terabit-per-second transmission. *Optica* **9**(1), 61 (2022) [arXiv:2108.01873](https://arxiv.org/abs/2108.01873). <https://doi.org/10.1364/OPTICA.449691>
- [38] Dang, S., Amin, O., Shihada, B., Alouini, M.-S.: What should 6G be? *Nature Electronics* **3**(1), 20–29 (2020) [arXiv:1906.00741](https://arxiv.org/abs/1906.00741). <https://doi.org/10.1038/s41928-019-0355-6>
- [39] Corcoran, B., Tan, M., Xu, X., Boes, A., Wu, J., Nguyen, T.G., Chu, S.T., Little, B.E., Morandotti, R., Mitchell, A., Moss, D.J.: Ultra-dense optical data transmission over standard fibre with a single chip source. *Nature Communications* **11**(1), 2568 (2020). <https://doi.org/10.1038/s41467-020-16265-x>
- [40] Chang, L., Liu, S., Bowers, J.E.: Integrated optical frequency comb technologies. *Nature Photonics* **16**(2), 95–108 (2022). <https://doi.org/10.1038/s41566-021-00945-1>
- [41] Kashiwazaki, T., Takanashi, N., Yamashima, T., Kazama, T., Enbutsu, K., Kasahara, R., Umeki, T., Furusawa, A.: Continuous-wave 6-dB-squeezed light with 2.5-THz-bandwidth from single-mode PPLN waveguide. *APL Photonics* **5**(3), 036104 (2020). <https://doi.org/10.1063/1.5142437>

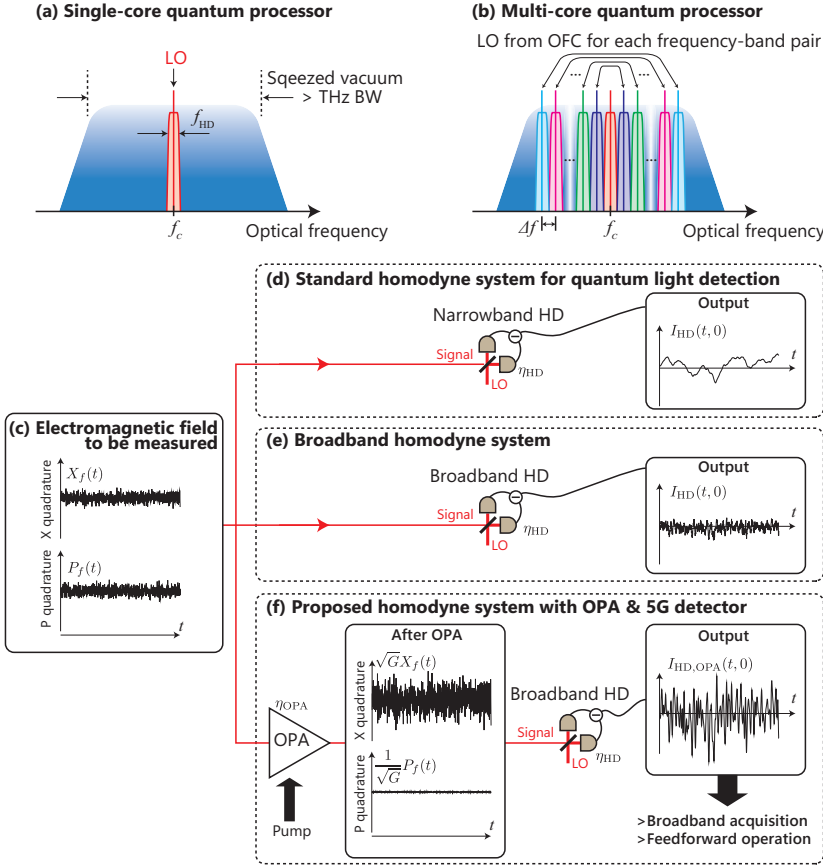


Fig. 1 (a) Bandwidth (BW) relationship between squeezed vacuum and homodyne detector. f_c , center frequency of the squeezed vacuum; f_{HD} , cut-off frequency of the homodyne detector; LO, local oscillator. (b) Concept of a multi-core quantum processor. Δf , frequency spacing. (c) Quadrature-phase amplitudes $X_f(t)$, $P_f(t)$ of the electromagnetic field of light to be measured with the temporal mode function $f(t)$. (d-f) Three kinds of homodyne apparatus measuring the X component ($\theta = 0$). Each $I_{HD}(t, 0)$ shows the output signal. The output signals are affected by the detection efficiencies and the bandwidths. (d) Standard homodyne system for quantum light detection. The photodiodes used in the homodyne detector have almost unity detection efficiencies, but the system bandwidth f_{HD} is typically less than a GHz. (e) Homodyne system with broadband balanced detector, which is often used in 5G applications. The bandwidth f_{HD} is beyond a GHz but the system efficiency is not high (typically $\sim 50\%$). (f) Proposed homodyne system with an OPA and a balanced detector for 5G applications. The X component of the input light field is amplified by the OPA excited by the pump light and is detected by the homodyne detector with the 5G balanced detector.

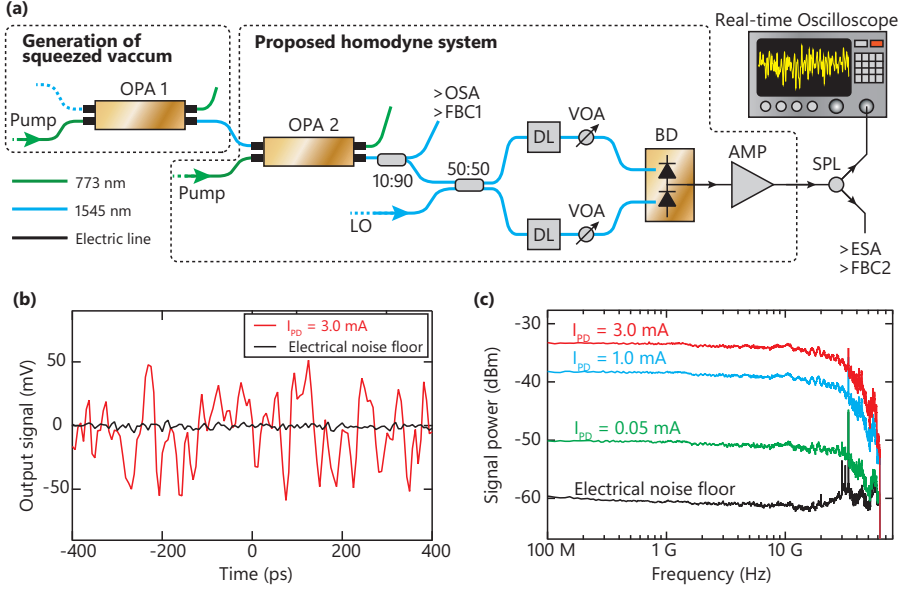


Fig. 2 (a) Experimental apparatus of the real-time quadrature phase amplitude measurement using the proposed homodyne system. OPA 1, optical parametric amplifier used for generating squeezed vacuum; OPA 2, optical parametric amplifier for amplifying the X component of the light to be measured; 10:90 and 50:50, fiber-based beamsplitters with coupling ratios of 90% and 50%, respectively; LO, local oscillator light (1545 nm); Pump, pump light for the OPAs (773 nm); VOAs, variable optical attenuators; DLs, optical delay lines; BD, balanced photodiode with a bandwidth of 43 GHz; AMP, broadband amplifier; SPL, broadband power splitter; OSA, optical spectrum analyzer; ESA, electrical spectrum analyzer, FBC1, feedback circuit for locking the phase among the squeezed vacuum and the pump light at OPA2; FBC2, feedback circuit for locking the phase at the amplified signal and LO. (b) Output signals measured by a real-time oscilloscope. The black trace shows the electrical noise floor when all lights are blocked. The red trace shows the shot noise of the LO when the photocurrent of a single photodiode is 3.0 mA. (c) Frequency responses of several photocurrents calculated by fast Fourier transformation of the oscilloscope data.

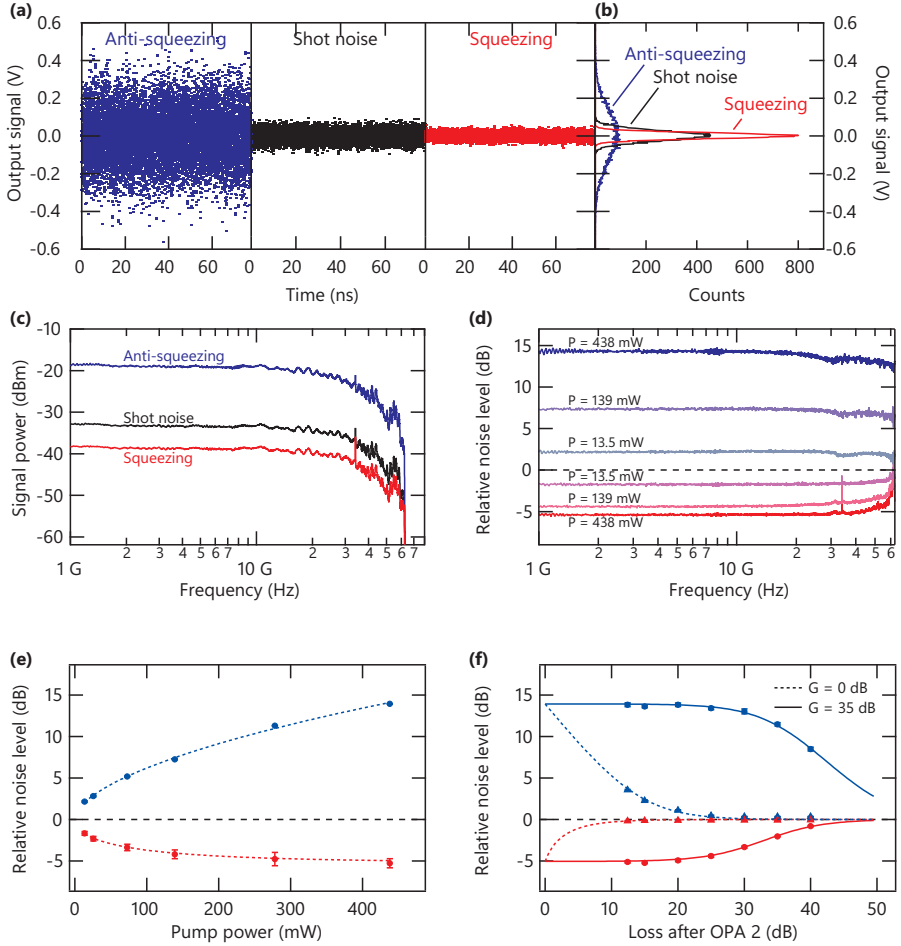


Fig. 3 Measurement results of the broadband squeezed vacuum. (a) Raw data acquired by the oscilloscope. Each point represents the quadrature phase component. (left) Anti-squeezing. (center) Shot noise. (right) Squeezing. (b) Histograms calculated from (a). (c) Frequency domain data calculated by FFT from the time-domain data. Each trace is averaged for 8192 frames of 12512 points of data. The pump power for OPA 1 is 438 mW. (d) Relative squeezing and anti-squeezing levels in the frequency domain for several pump powers. (e) Pump-power dependence of the squeezing (red circles) and anti-squeezing (blue circles) levels. The dashed lines show fitting results. (f) Calculated (lines) and measured (markers) squeezing levels with additional loss after OPA2. The gain of OPA2 was set to 0 dB (dashed lines) and 35 dB (solid lines).